Philippine Journal of Science
146 (4): 395-402, December 2017
ISSN 0031 - 7683
Date Received: 10 Aug 2016

Hydrothermal Synthesis of Hierarchical Hematite (α-Fe_2O_3) Microstructures for Photocatalytic Degradation of Methyl Orange

Nick Joaquin Rapadas and **Mary Donnabelle L. Balela**

Sustainable Electronic Materials Group
Department of Mining, Metallurgical, and Materials Engineering
University of the Philippines Diliman, Quezon City 1101, Metro Manila, Philippines

Hematite (α-Fe_2O_3) hierarchical microstructures were prepared by a simple and inexpensive hydrothermal method using a mixture of $FeCl_3$ and Na_2SO_4 as precursors, followed by annealing at 400° C for 2 h. α-Fe_2O_3 microspheres with an average diameter of 1.07 µm were formed in the solution. Microrods with an average length of 0.46 µm were also observed on the surface of the microspheres, forming an urchin-like morphology. The amounts of Fe^{3+} and $(SO_4)^{2-}$ in the solution significantly influence the morphology of the α-Fe_2O_3 urchin-like microstructures. An optimum amount of Fe^{3+} and $(SO_4)^{2-}$ leads to the formation of urchin-like microstructures. The α-Fe_2O_3 microstructures successfully degraded methyl orange after 1 h of UV irradiation in the presence of a minute amount of hydrogen peroxide (H_2O_2). The α-Fe_2O_3 microstructures also exhibit excellent reusability and stability making it an ideal photocatalyst for wastewater treatment.

Keywords: dye, hematite, hierarchical microstructures, hydrothermal treatment, photocatalyst

INTRODUCTION

The use of iron oxide nanomaterials, particularly hematite, is prevalent in various fields due to potential applications, such as gas sensing (Abe et al. 1997, Zhang et al. 2009), wastewater treatment (Hua et al. 2012), photocatalysis (Verhoeven 1996, Mishra & Chun 2015), photovoltaics (Gotić et al. 2011), field-emission (FE) devices (Hsu et al. 2011), and glucose sensing (De Mesa et al. 2011). Thus, different synthesis methods for iron oxide nanomaterials have been studied extensively. In particular, hematite (α-Fe_2O_3) nano and microstructures are promising photocatalysts. Substantial efforts have already been made to prepare α-Fe_2O_3 with various morphologies (Atabaev, 2015). Examples include nanowires (Chirita & Grozescu 2009), nanorings (Mohapatra & Anand 2010), hollow spheres (Yu et al. 2009), nanorods and capsules (Sun et al. 2012). The physical and chemical properties of α-Fe_2O_3 nano and microstructures are influenced by the morphology. Thus, much research has been focused on controlling the morphology, as well as in the fabrication of complex structures. For example, in hydrothermal synthesis, the morphology of the α-Fe_2O_3 microstructures is strongly affected by the presence of inorganic anions in the solution. By changing the concentration of inorganic anions, the shape and size of the α-Fe_2O_3 microstructures can be easily varied, without introducing any impurities in the product (Gotić et al. 2011).

Recently, the focus of photocatalytic applications has been on environmental remediation and water splitting applications. Photocatalysts are employed to degrade harmful organic substances using UV and visible light (Gotić et al. 2011). Various industries, such as textile,

*Corresponding author: mlbalela1@up.edu.ph

leather goods, food, polymers, and cosmetics make use of organic compounds, which then becomes pollutants when discarded as wastewater. Most of these organic pollutants consist of dyes which have been proven to be carcinogenic. Consequently, the removal of these pollutants through photodegradation is of distinct importance (Guo et al. 2011). Different metal oxides e.g., titanium oxide (TiO_2), zinc oxide (ZnO), tin oxide (SnO_2) and α-Fe_2O_3, are found to effective in degrading organic pollutants under UV and visible light. Compared to these oxides, α-Fe_2O_3 offers several advantages, such as abundance, ease of preparation, narrow band gap, and excellent chemical stability under irradiation (Liu et al. 2015).

In this work, the formation of hierarchical α-Fe_2O_3 microstructures by hydrothermal method is presented. The effects of the concentration of the reactants i.e., $FeCl_3$ and Na_2SO_4, in controlling the morphology of the resulting microstructures are investigated. The efficacy of the as-prepared α-Fe_2O_3 microstructures in the photocatalytic degradation of methyl orange − in the presence of a small amount of hydrogen peroxide − is also examined.

MATERIALS AND METHODS

Hydrothermal Synthesis of Hematite Microstructures

Hematite microstructures were prepared based on the work of Agarwala et al. 2012, with minor modifications in the drying temperature (60-80° C) and annealing ramp rate (1-2° C min^{-1}). In a typical experiment, 2 mmol iron chloride ($FeCl_3.6H_2O$, Sigma Aldrich, 99.99%) and 2 mmol sodium sulfate (Na_2SO_4, Sigma Aldrich, 99.99%) were added into 40 mL deionized water and stirred until totally dissolved. The solution was heated in an autoclave at 120° C for 6 h and then cooled to room temperature. The products were collected by centrifugation and washed with de-ionized (DI) water and ethanol several times and later dried in air at 80° C for 2 h. The as-prepared powder was annealed in air at 400° C for 2 h with a ramp-rate of 2° C min^{-1} to convert to α-Fe_2O_3.

To determine the effect of the concentration of Fe^{3+} and SO_4^{2-} ions on the morphology of the microstructure, various samples with different concentrations of $FeCl_3$ and Na_2SO_4 were made while keeping the concentration of either $FeCl_3$ or Na_2SO_4 constant. The concentrations of the synthesized samples are shown below:

Table 1. Sample Concentrations ($FeCl_3$: constant).

Concentration of $FeCl_3$	Concentration of Na_2SO_4		
	1 mmol	2 mmol	4 mmol
2 mmol	Sample A	(1:1 Ratio) Sample B	Sample C

Table 2. Sample Concentrations (Na_2SO_4: constant).

Concentration of Na_2SO_4	Concentration of $FeCl_3$		
	2 mmol	4 mmol	12 mmol
2 mmol	(1:1 Ratio) Sample D	Sample E	Sample F

Characterization of Hematite Microstructures

The morphology of the microstructures was observed using a scanning electron microscope (SEM, Hitachi TM 1000, Jeol JSM-5310). The mean diameters of the microstructures and the length of the microrods were estimated by measuring 100 individual spheres and rods from several SEM images using Image Analysis and Processing in Java (ImageJ) software. X-ray diffraction (XRD, Shimadzu 7000) was used to analyze the crystal structure and phase composition of the product using Cu *K*α radiation.

Photocatalytic Degradation of Methyl Orange

The photocatalytic properties of the synthesized α-Fe_2O_3 microstructures were determined through the time-dependent photocatalytic degradation of methyl orange (MO). 30 mg of the α-Fe_2O_3 microstructures were added to 30 mL of 5 ppm MO solution. The solutions were then magnetically stirred in the dark for 30 min to allow equilibrium to occur. After stirring, 0.15 ml of H_2O_2 (J. Chemie, 3% USP 10 vol) was added to the MO and α-Fe_2O_3 solution. Photocatalytic degradation of 5 ppm MO was then performed by irradiation under 30 W UV lamp at specific time intervals (0, 15, 30, 45, 60, 75, 90 min). The degradation of MO was investigated by determining the change in the absorbance of the 5 ppm MO solution at the peak (~465 nm) for every time interval using UV-visible spectrophotometer (UV-VIS, Shimadzu UV-1700 PharmaSpec).

RESULTS AND DISCUSSION

Effects of Na_2SO_4 and $FeCl_3$ Concentration on the Formation of Hematite Microstructures

The effect of Na_2SO_4 concentration on the morphology of the α-Fe_2O_3 microstructures was first investigated. The amount of $FeCl_3$ was kept constant at 2 mmol and all other experimental parameters like temperature and reaction time were also kept constant. On the other hand, the concentration of Na_2SO_4 was varied from 1, 2, and 4 mmol. Figure 1 shows the SEM images of α-Fe_2O_3 microstructures at increasing $(SO_4)^{2-}$ ion concentration. When 1 mmol Na_2SO_4 was added, clusters of microrods with an average length of 0.56 ± 0.04 μm were formed.

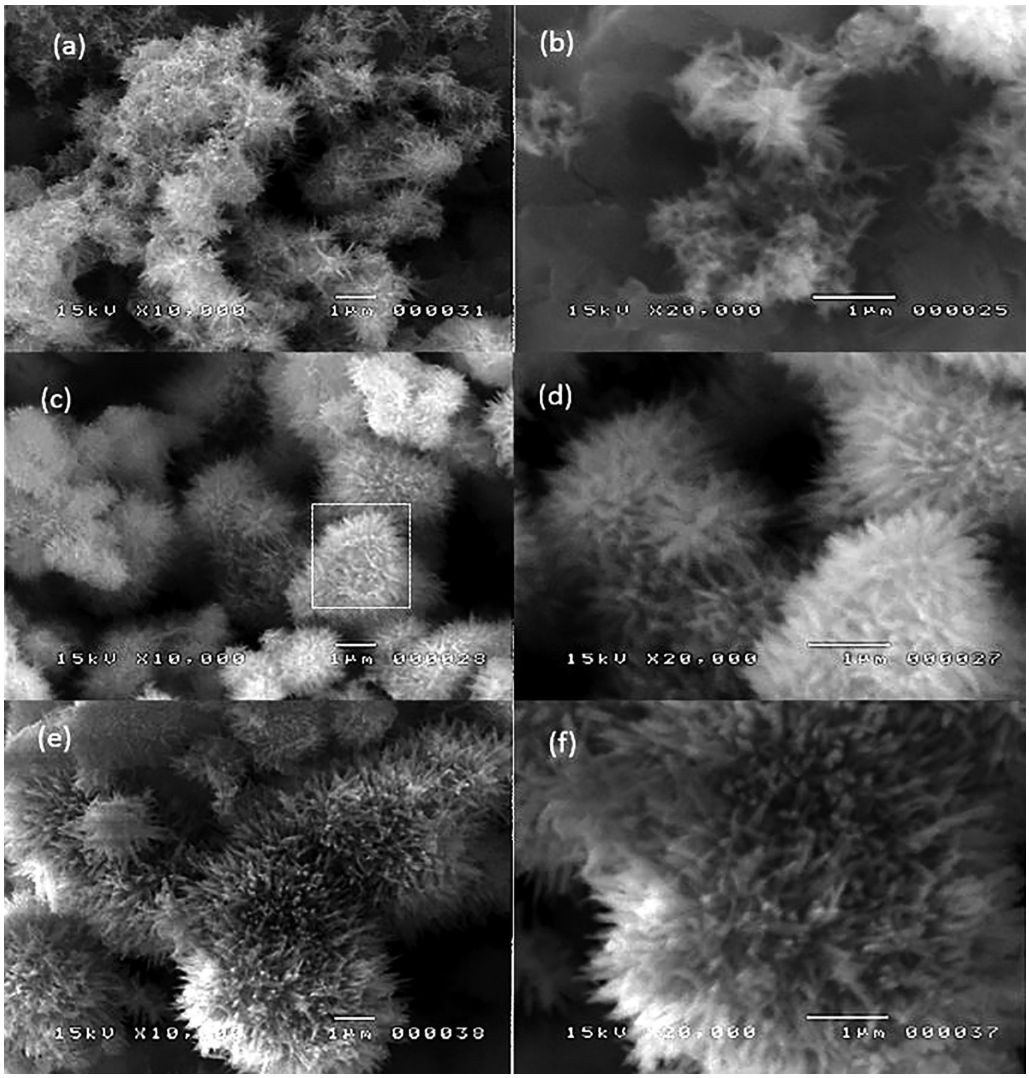

Figure 1. SEM images showing the morphology of the hematite hierarchical microstructures formed at a,b) 1 mmol; c,d) 2 mmol; and e,f) 4 mmol Na_2SO_4 concentration at 10,000X and 20,000X magnification with Fe^{3+} ion concentration held constant at 2 mmol. Box on Fig 1c shows the area of the sample magnified in Fig. 1d.

It is apparent from the high magnification SEM image in Fig. 1b that these microrods grew from a single microsphere with a mean diameter of about 0.35 ± 0.02 µm. This microsphere possibly serves as nucleation point for the microrods. At higher magnification, some microrods also appeared to be loose aggregates as seen in Fig. 1b.

At 2 mmol Na_2SO_4, hierarchical microstructures with urchin-like morphology (Fig. 1c and d) were produced. The microspheres, which acted as seed for the growth of the microrods, have an average diameter of 1.07 ± 0.03 µm. On the other hand, the mean length of the microrods decreases to about 0.46 ± 0.03 µm. Increasing the Na_2SO_4 concentration to 4 mmol formed larger microspheres with similar urchin-like morphology (Fig. 1e and f). The average diameter of these structures is around 2.38 ± 0.01 µm. However, the microrods comprising the urchin-like structures decrease in length, with an average length of 0.42 ± 0.03 µm.

On the other hand, the effect of $FeCl_3$ concentration on the morphology of the product was also studied. The amount of Na_2SO_4 was kept constant at 2 mmol and all other experimental parameters like temperature and reaction time were also kept constant. The $FeCl_3$ concentration was changed from 2, 4, and 12 mmol. Figure 2 shows the SEM images of hematite microstructures formed by hydrothermal synthesis with 2, 4, and 12 mmol $FeCl_3$ concentration at a constant Na_2SO_4 concentration of 2 mmol. Addition of 2 mmol $FeCl_3$ generated large microspheres with an urchin-like morphology (Fig. 2a and b). This powder was prepared at the same condition as the sample shown in Fig. 1c and d. The microspheres

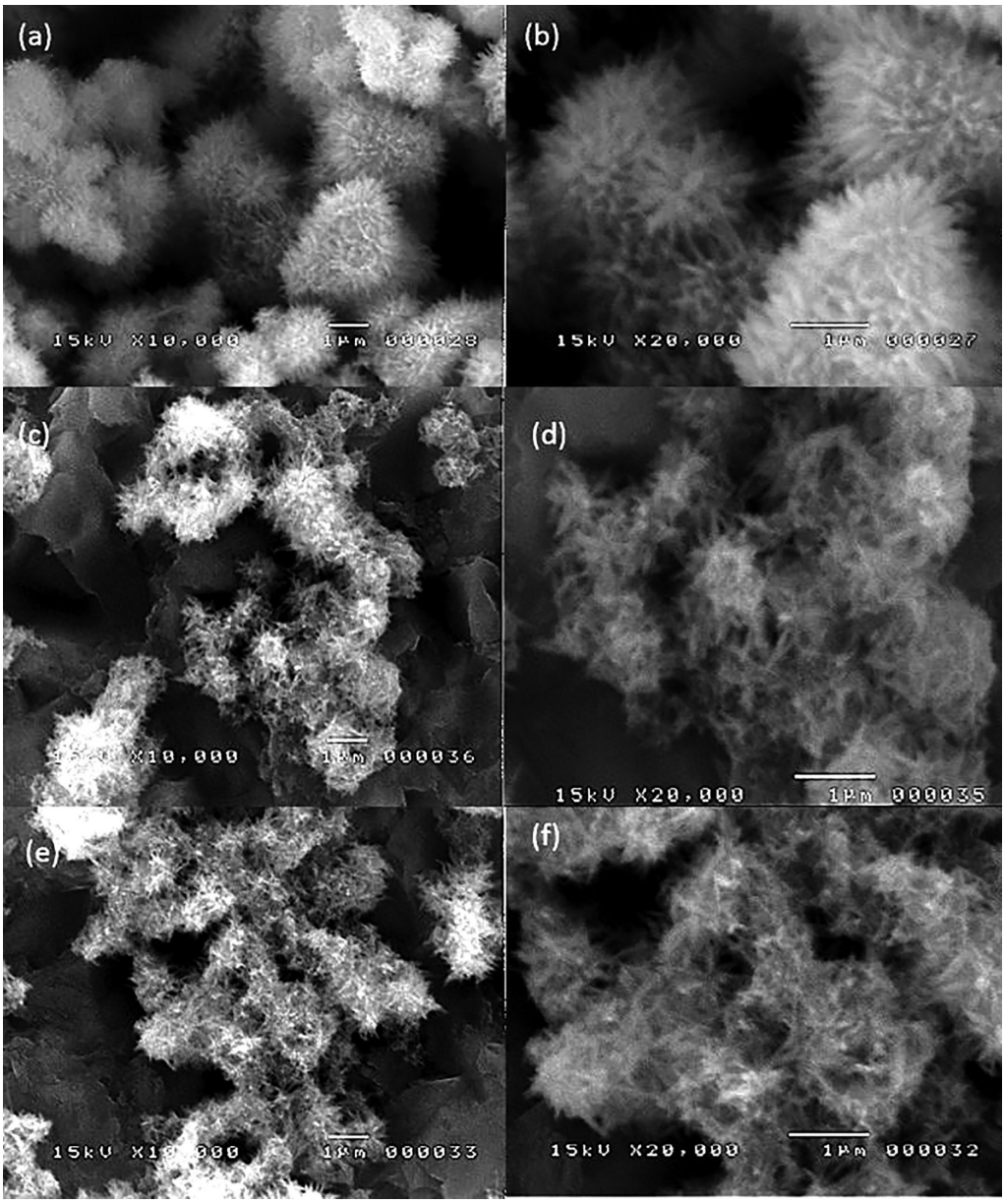

Figure 2. SEM images showing the morphology of the hierarchical hematite microstructures formed at a,b) 2 mmol; c,d) 4 mmol; and e,f) 12 mmol Fe^{3+} ion concentration at 10,000X and 20,000X magnification with SO_4^{2-} ion concentration held constant at 2 mmol.

have an average diameter of 1.07 ± 0.03 µm, while the nanorods with an average length of 0.46 ± 0.03 µm. Both the 4 and 12 mmol $FeCl_3$ concentrations formed only clusters of microrods with an average length of 0.40 ± 0.03 µm. Compared to the urchin-like particles in Fig. 2a-b, the microrods do not appear to grow from a spherical seed.

Based on the SEM images in Fig. 1 and 2, it is obvious that both Fe^{3+} and $(SO_4)^{2-}$ concentrations significantly influenced the morphology of the hematite microstructrues. During hydrothermal reaction Fe^{3+} ions are hydrolyzed to form the intermediate phase FeOOH (Xie et al. 2009, Zeng et al. 2010, Agarwala et al. 2012). This material serves as the precursor for the formation of hematite. At the early stages of the hydrothermal reaction, FeOOH nucleates in the solution and subsequently agglomerates to form large microspheres (Xie et al. 2009, Zeng et al. 2010, Agarwala et al. 2012). Due to the acidic nature of the solution, Fe^{3+} ions are drawn towards the surface of the nuclei, which then leads to the attraction of $(SO_4)^{2-}$ ions. The alternate adsorption of Fe^{3+} and $(SO_4)^{2-}$ ions results to the formation of the Fe-O-SO_2-O-Fe bidentate structure, which attaches on the surface parallel to the c-axis of the FeOOH nuclei

(Xie et al. 2009, Zeng et al. 2010, Agarwala et al. 2012). Subsequently, the microrods are grown. Finally, the FeOOH nuclei with the bidentate branches are converted to hematite urchin-like microstructures after the subsequent annealing of the collected powder.

It is known that $(SO_4)^{2-}$ ions strongly complexes with Fe^{3+} (Xie et al. 2009, Zeng et al. 2010, Agarwala et al. 2012). When low amounts of $(SO_4)^{2-}$ ions are present in the solution, the nucleation of the FeOOH is possibly slower, leading to smaller microspheres (Xie et al. 2009, Zeng et al. 2010, Agarwala et al. 2012). This then favors the formation of the Fe-O-SO_2-O-Fe bidentate structure and the subsequent growth of the microrods. As a result, longer microrods are present on the surface of the microspheres as seen in Fig. 1a and b. Increasing the $(SO_4)^{2-}$ ion concentration promotes the precipitation of FeOOH, which produces larger and more defined microspheres. As a consequence, the length of the microrods noticeably decreases from 0.56 ± 0.04 μm to 0.42 ± 0.03 μm as amount is increased from 1 mmol Na_2SO_4 to 4 mmol Na_2SO_4. On the other hand, it is possible the hydrolysis reaction and subsequent formation of FeOOH is slowed down at higher amount of Fe^{3+} ions (Xie et al. 2009, Zeng et al. 2010, Agarwala et al. 2012). This condition is advantageous for the oriented growth of the microrods as time is needed for the formation of the Fe-O-SO_2-O-Fe bidentate structure.

Photocatalytic Degradation of Methyl Orange

The various morphologies of the hematite samples used in the photodegradation experiments are shown in Figure 3. The samples represent small, medium, and relatively larger sized hematite microstructures to elucidate the effect of morphology on the photocatalytic activity of the microstructures. The photocatalytic activity of these hematite microstructures for methyl orange (MO) degradation was evaluated in the presence of a very small amount of H_2O_2. Figure 4 shows the UV-Vis absorption spectra of methyl orange, with hematite microstructures (sample A) and H_2O_2 only, and H_2O_2 with the different hematite microstructures after exposure to UV light for 1 h. The methyl orange solution registered an absorbance peak at around 465 nm as seen in Fig. 4a. For all other samples, no significant peak shift or presence of any other peak was observed, indicating that the solution collected after UV irradiation remained methyl orange. After 1 h UV irradiation with hematite only (sample A), the UV-Vis peak was unchanged as shown in Fig. 4b. This suggests that no photodegration of methyl orange occurred. In the presence of minute amount of H_2O_2, a significant decrease in absorbance of about 57% can be observed even without the presence of hematite (Fig. 4c). This can be attributed to the generation of hydroxyl radicals when H_2O_2 is exposed to UV light (Yu et al. 2009).

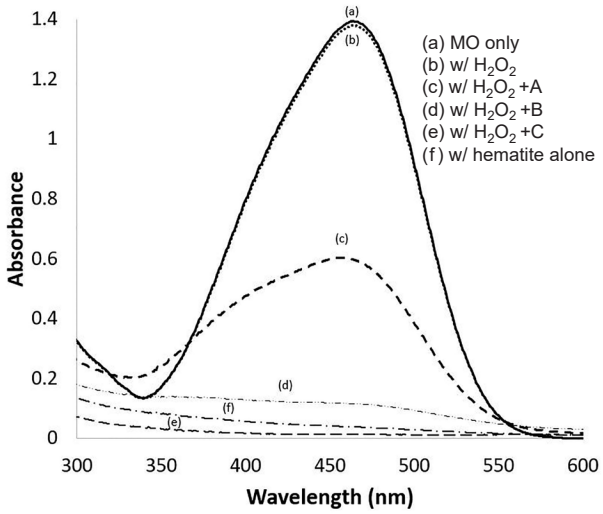

Figure 4. UV-is absorption spectra of (a) methyl orange, (b) methyl orange with hematite sample A only, (c) methyl orange with H_2O_2 only, (d) methyl orange with H_2O_2 and hematite sample A, (e) methyl orange with H_2O_2 and hematite sample B, and (f) methyl orange with H_2O_2 and hematite sample C after exposure to UV light for 1 h.

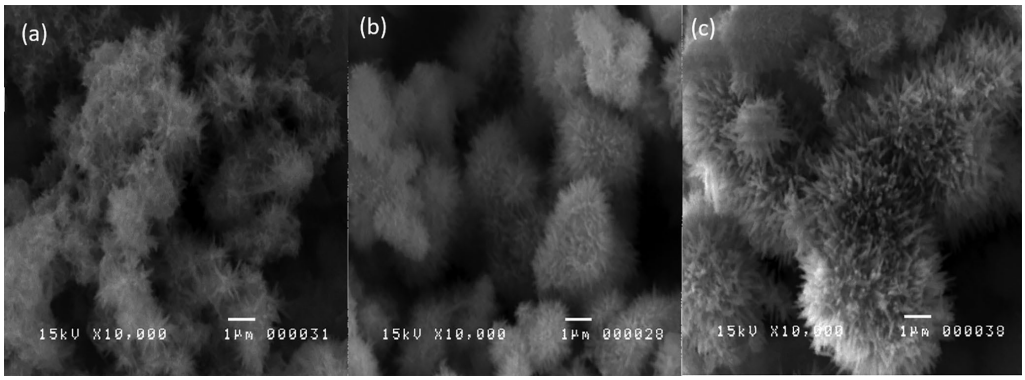

Figure 3. SEM images showing the morphology of hematite microstructures used for photocatalytic degradation of methyl orange (a) A, (b) B, and (c) C at 10,000X magnification.

Then again, an almost complete photodegradation of methyl orange was observed when both hematite microstructures and H_2O_2 were present in the solution (Fig. 4d-f). The increase in the photocatalytic activity can be explained by the following mechanism. Due to UV irradiation, α-Fe_2O_3 generates electron-hole pairs. The photogenerated electrons are ejected from the valence band of α-Fe_2O_3 to its conduction band, leaving behind a hole in the valence band (Equation 1).

$$Fe_2O_3 \rightarrow Fe_2O_3 (e_{cb}^-, h_{vb}^+) \quad (1)$$

The photogenerated electrons may either: (a) react with H_2O_2 to form highly reactive hydroxyl (OH) radicals (Yu et al. 2009),

$$e_{cb}^- + H_2O_2 \rightarrow OH^- + \cdot OH \quad (2)$$

or (b) react with the surface of the catalyst (Fe^{3+}) to produce Fe^{2+}, which will further react with H_2O_2 to generate the Fenton's reagent (Yu et al. 2009).

$$Fe^{3+} + e_{cb}^- \rightarrow Fe^{2+} \quad (3)$$

$$Fe^{2+} + H_2O_2 \rightarrow Fe^{3+} + OH^- + \cdot OH \quad (4)$$

The generation of highly reactive hydroxyl (OH) radicals in Equation 2 and 4 are able to degrade the methyl orange dye into non-toxic organic compounds due to their strong oxidizing ability (Yu et al. 2009, Liu et al. 2015). However, Equation 3 and 4 indicates that the reaction is highly likely to start on the surface of the hematite microstructures, starting with the reduction of Fe^{3+} to Fe^{2+}, which is then released into the solution. The free Fe^{2+} ions will then react with the H_2O_2, to form the Fenton's reagent which serves as a trigger for the photocatalytic degradation of the methyl orange (Araujo et al. 2011). The Fenton reaction is considered to be a potent advanced oxidation process for wastewater treatment and is used to destroy organic compounds (Yu et al. 2009).

Figure 5 shows the photocatalytic activity of hematite microstructures in the presence of H_2O_2 with increasing irradiation time. A plot for H_2O_2 alone is also seen on the graph. Co and C are the initial and actual concentration of methyl orange after UV irradiation, respectively. The photocatalytic degradation of the methyl orange agrees with the pseudo-first order kinetics since the R^2 coefficients for the photocatalytic activity of the hematite microstructures show a good fit with R^2 values ranging from 0.928 to 0.976. The pseudo first order rate constant (k) of methyl orange with only H_2O_2, and H_2O_2 with hematite samples A, B, and C, under UV irradiation was calculated to be about 0.0265, 0.0499, 0.0577, and 0.0563 min^{-1}, respectively. The photocatalytic activity of the hematite samples (A, B, C) were found to be

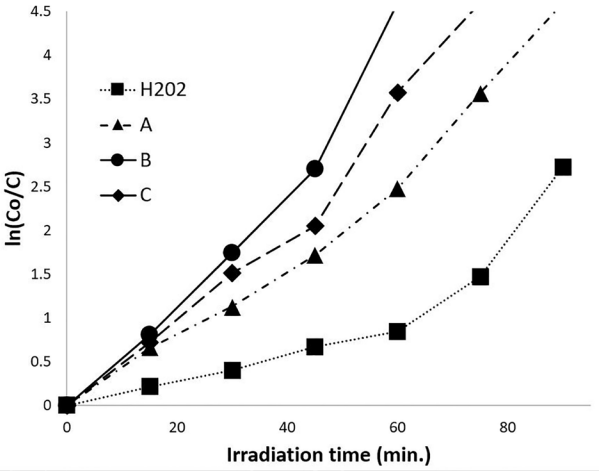

Figure 5. Comparison of the photocatalytic activity of various hematite hierarchical microstructures for the photodegradation of methyl orange in the presence of H_2O_2. A plot for the photocatalytic activity for H_2O_2 alone is also shown.

significantly higher than the activity of H_2O_2 alone based on the calculated rate constants. With hematite sample A, B, and C having more than 46.89%, 54.07%, and 52.93% increase in photocatalytic activity compared to H_2O_2 alone, respectively.

Hematite sample B was found to be slightly higher than sample C in terms of photocatalytic activity, with sample A being the least active. Sample A lags behind the two microstructures since it is composed of clusters of microrods that may have assembled together to form loose aggregates, therefore it lacks the hierarchical microstructure present in samples B, and C. The urchin-like structures of samples B and C may have more efficient means of transport for the electrons to move to the active sites on the surface, thus leading to an improved efficiency for the photocatalytic reactions. The high photocatalytic activity of sample B may be attributed to its high surface area and smaller size compared to sample C which has a significantly bigger diameter (Yu et al. 2009).

Figure 6 shows the XRD pattern of the hematite microstructures before and after 5 cycles of use in the complete degradation of MO. Both XRD patterns shows major peaks at 2θ = 33.2°, 35.66 °, 54.14, and 64.08°. These peaks correspond to the 104, 110, 116, and 300 peaks of α-Fe_2O_3. The minor peaks of α-Fe_2O_3 are found at 2θ= 24.16°, 40.9°, 49.52°, 57.66°, and 62.5°. These minor peaks correspond to 012, 113, 024, 018, and 214 peaks respectively. All the diffraction peaks in both patterns can be indexed to the standard diffraction pattern of a rhombohedral α-Fe_2O_3 (hematite, JCPDS no. 33-0664), indicating that the product is pure hematite without the presence of any impurities. Even after 5

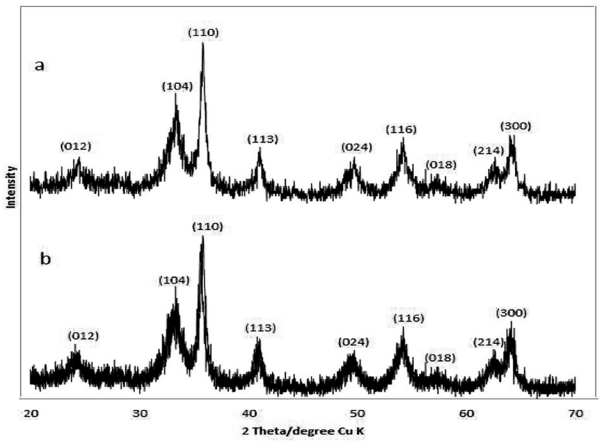

Figure 6. XRD patterns of (a) hematite microstructure formed after annealing at 400° C for 2 h and (b) hematite microstructures after 5 cycles of uses in the photocatalytic degradation of MO.

cycles of use, the α-Fe_2O_3 peaks remain unchanged as seen in Fig. 6b. No other phases were formed.

Overall, the hematite microstructures formed in this study can be considered as an ideal photocatalyst due to its distinct degradation of the methyl orange dye, its photostability and reusability. The presence of H_2O_2 in the system will enhance the effectiveness of the hematite catalyst through the Fenton reaction. Additionally, H_2O_2 can be easily degraded by the aqueous couple Fe^{2+}/Fe^{3+}, which eliminates issues of H_2O_2 contamination (Guo et al. 2011). The catalysts can also be used in the industrial scale since they can be separated more easily from the slurry system through filtration or sedimentation after treatment due to their larger weight/size, and weaker Brownian motion when compared to conventional powders of micro-sized photocatalytic materials (Araujo et al. 2011).

CONCLUSIONS

Hematite (α-Fe_2O_3) microstructures were successfully formed using only $FeCl_3$ and Na_2SO_4 as precursors, with the use of low temperature hydrothermal synthesis and an annealing process at 400° C. In the formation of the hematite microstructures, the amounts of Fe^{3+} and $(SO_4)^{2-}$ ions significantly influenced the resulting morphology and size. Furthermore, the photocatalytic activity of the hematite microstructures could be adjusted by tailoring its morpholgy. The prepared hematite microstructures show significant photocatalytic activity for the degradation of methyl orange. The H_2O_2 treatment only yielded a photocatalytic reaction rate of 0.0265 min^{-1} while the urchin-like hematite microstructure with the highest photocatalytic activity yielded 0.0577 min^{-1}, signifying a 54.07% increase in photocatalytic activity compared to H_2O_2 treatment alone. The outstanding photocatalytic properties of the urchin-like hematite microstructures could be attributed to their morphology, where it provides more efficient active sites. Consequently, there is an increase in electron transport properties, thus leading to an improved efficiency for the photocatalytic reactions. The hematite microstructures showed excellent stability and reusability after 5 cycles of complete degradation of methyl orange.

ACKNOWLEDGMENT

The project is partially funded by the University of the Philippines System under the Office of the Vice-President for Academic Affairs for the Emerging Interdisciplinary Research (OVPAA-EIDR-C06-032). The authors wish to thank Mr. Luigi Dahonog for the assistance in editing this manuscript.

Conflict of Interest

The authors have no conflict of interest.

REFERENCES

ABE R, SHINOHARA K, TANAKA A, HARA M, KONDO JN, DOMEN K . 1997. Preparation of porous niobium oxides by soft-chemical process and their photocatalytic activity. Chemistry of Materials 9(10):2179-2184 .

AGARWALA S, LIM ZH, NICHOLSON E, HO GW. 2012 . Probing the morphology-device relation of Fe_2O_3 nanostructures towards photovoltaic and sensing applications. Nanoscale 4(1):194-205

ARAUJO FVF, YOKOYAMA L, TEIXEIRA LAC, CAMPOS JC. 2011 . Heterogeneous fenton process using the mineral hematite for the discolouration of a reactive dye solution. Brazilian Journal of Chemical Engineering 28(4):605-616.

ATABAEV TSJ. 2015. Facile hydrothermal synthesis of flower-like hematite microstructure with high photocatalytic properties. Journal of Advanced Ceramics 4(1):61-64.

CHIRITA M, GROZESCU I. 2009. Fe_2O_3 – Nanoparticles, physical properties and their photochemical and photoelectrochemical applications. Chem. Bull. "POLITEHNICA" Univ. (Timişoara) 54(68):1-8.

DE MESA DM, SANTOS GNC, QUIROGA RV. 2011. Synthesis and characterization of Fe_2O_3 nanomaterials using HVPC growth technique for glucose sensing application. International Journal of Scientific &

Engineering Research 3(8):1-8.

GOTIĆ M, DRAŽIC G, MUSIĆ S . 2011. Hydrothermal synthesis of α-Fe_2O_3 nanorings with the help of divalent metal cations, Mn^{2+}, Cu^{2+}, Zn^{2+} and Ni^{2+}. Journal of Molecular Structure 993(1-3):167-176.

GUO P, WEI Z, WANG B, DING Y, LI H, ZHANG G, ZHAO XS. 2011. Controlled synthesis, magnetic and sensing properties of hematite nanorods and microcapsules. Colloids and Surfaces A: Physicochemical and Engineering Aspects 380(1-3):234-240.

HSU L-C, YU H-C, CHANG T-H, LI Y-Y. 2011. Formation of three-dimensional urchin-like α-Fe_2O_3 structure and its field-emission application. ACS Applied Materials and Interfaces 3(8):3084-3090.

HUA M, ZHANG S, PAN B, ZHANG W, LV L, ZHANG Q. 2012. Heavy metal removal from water/wastewater by nanosized metal oxides: A review. Journal of Hazardous Materials 211-212:317-331.

LIU X, CHEN K, SHIM J-J, HUANG J. 2015. Facile synthesis of porous Fe_2O_3 nanorods and their photocatalytic properties. Journal of Saudi Chemical Society 19(5):479-484.

MISHRA M, CHUN D-M. 2015. α-Fe_2O_3 as a photocatalytic material: A review. Applied Catalysis A: General 498:126-141.

MOHAPATRA M, ANAND S. 2010. Synthesis and applications of nano-structured iron oxides/hydroxides-a review. International Journal of Engineering, Science and Technology 2(8):127-146 .

SUN P, WANG W, LIU Y, SUN Y, MA J, LU J. 2012. Hydrothermal synthesis of 3D urchin-like α-Fe_2O_3 nanostructure for gas sensor. Sensors and Actuators B: Chemical 173:52-57.

VERHOEVEN JW. 1996. Glossary of terms used in photochemistry. Pure & Appl. Chem 68(12):2223-2286.

XIE X, YANG H, ZHANG F, LI L, MA J, JIAO H, ZHANG J. 2009. Synthesis of hollow microspheres constructed with α-Fe_2O_3 nanorods and their photocatalytic and magnetic properties. Journal of Alloys and Compounds, 477:90-99.

YU J, YU X, HUANG B, ZHANG X, DAI Y. 2009. hydrothermal synthesis and visible-light photocatalytic activity of novel cage-like ferric oxide hollow spheres. Cryst. Growth Des. 9(3):1474-1480.

ZENG S, TANG K, LI T, LIANG Z. 2010. Hematite with the urchinlike structure: its shape-selective synthesis, magnetism, and enhanced photocatalytic performance after TiO_2 encapsulation. Journal of Physical Chemistry C. 114:274-283

ZHANG F, YANG H, XIE X, LI L, ZHANG L, YU J, ZHAO H, LIU B. 2009. Controlled synthesis and gas-sensing properties of hollow sea urchin-like hematite nanostructures and hematite nanocubes. Sensors and Actuators B: Chemical 141:381-389.